한국기계가공학회지, 제19권, 제4호, pp.16～23(2020.04) ISSN 1598-6721(Print)
Journal of the Korean Society of Manufacturing Process Engineers, Vol. 19, No. 4, pp.16~23(2020.04) ISSN 2288-0771(Online)

https://doi.org/10.14775/ksmpe.2020.19.04.016

Analysis of Heat Treatment Process Conditions for Output Characteristics of Permalloy Core on Current Sensors using DOE

Young Shin Kim*, Yoon Sang Kim**, Euy Sik Jeon***,#

*Industrial Technology Research Institute, Kongju National UNIV., **R & D Center, Vision Technologies., ***Department of Mechanical & Automotive Engineering, Kongju National UNIV.

실험계획법을 이용한 퍼멀로이 전류 코어 센서의 출력특성에 관한 열처리 공정조건 분석

김영신*, 김윤상**, 전의식***,#

*공주대학교 생산기술연구소, **(주)비전테크놀러지 R&D센터, ***공주대학교 기계자동차공학부

(Received 9 March 2020; received in revised form 18 March 2020; accepted 25 March 2020)

ABSTRACT

An electric vehicle operates at high currents and requires real-time monitoring of the entire system for ensuring efficiency and safety of the vehicle. Current sensors are applied to drive the motors, inverters, and battery control systems, and are the key components to ensure constant monitoring of the magnitude and waveforms of the operating current. In this study, a heat treatment process condition to influence the performance of Permalloy current sensors was developed; the correlation between the output capacity, low-temperature characteristics, and high-temperature characteristics of the current sensor was studied; and the process was optimized to meet the required output accuracy and temperature characteristics.

Keywords: Current sensors(전류 센서), DOE(실험계획법), Heat treatment(열처리), Permalloy(퍼멀로이)

1. Introduction

Electric vehicles are commonly referred to as vehicles driven by batteries and electric motors [1-2]. The paradigm of the global automobile market is shifting from internal combustion engine cars to electric vehicles owing to the reinforced international environmental regulations on automobile exhaust and imminent oil depletion[3].

An electric vehicle comprises components, such as

Corresponding Author : osjun@kongju.ac.kr
Tel: +82-41-521-9284, Fax: 05051159284

a driving motor, a battery, and an inverter. It operates at high currents and requires real-time monitoring of the entire system for efficiency and safety of the vehicle to be ensured. This monitoring requires the measurement of high current and a high-performance current sensor to measure the high current[4]. Current sensors are applied to drive the motors, inverters, and battery control systems, and are the key components for the constant monitoring of the magnitude and waveforms of the operating current [5-6]. In general, the current sensors are broadly categorized into four types: shunt, CT and Hall sensor, open loop type, and close loop type using a magnetic core[7-8].

Among these, the Hall type current sensor is widely used to measure the current of a battery owing to its excellent output linearity, small size, and low cost. However, the performance of these current sensors is determined by the magnetic properties of the raw material and magnetic iron core material, coating conditions, iron core processing method, and hydrogen reduction heat treatment process. By changing the material of the sensor from a directional Si-steel material to a Permalloy material, the saturation point can be increased according to the material shape, and the sensitivity of the sensor itself can be significantly improved with high permeability. Additionally, the product shape does not have a significant influence on the performance of the sensor in the existing electrical steel sheet. however, the shape and processing method of the product are considerably important because the stress relief in the Permalloy material is a significantly important factor[9].

Therefore, in this study, a heat treatment process condition to influence the performance of Permalloy current sensors was developed; the correlation between the output capacity, low-temperature characteristics, and high-temperature characteristics of the current sensor was studied; and the process was optimized to meet the required output accuracy and temperature characteristics.

2. Heat Treatment Test

2.1 Test Method

The material used in this study was Permalloy (ASTM A753 Alloy Type 4), and heat treatment was performed on it to eliminate the residual stress caused by the rolling and manufacturing process employed for the steel sheet. During the hydrogen reduction heat treatment, when the temperature increased beyond 1,000 ℃, reduction reactions occurred with hydrogen and other impurities, such as oxygen, carbon, and sulfur in the material, thereby eliminating the impurities in the material more effectively. In this study, the annealing temperature was set to 1,100 ℃, and the reduction heat treatment conditions were adjusted by varying the amount of hydrogen introduced into the furnace. The test specimens were fabricated using high-speed presses with 0.1T 22.2×19.9×5 thread core specimens to analyze the output characteristics depending on the heat treatment molding conditions, using the hydrogen reduction heat treatment machine by producing ring-type core specimens.

2.2 Setting Variables

For the hydrogen reduction heat treatment of Permalloy material, high-temperature heat treatment was performed, followed by low-temperature heat treatment. Key process variables, such as the maintained temperature, retention time, and hydrogen concentration during annealing, were set. After performing the basic experiments on the process conditions for the high-temperature annealing process, including the maintained temperature, amount of hydrogen, and belt speed, and on the process conditions for the low-temperature heat treatment ordering, including the maintained temperature, amount of hydrogen, and belt speed, three process variables that have significant impacts on the experimental results were selected.

Table 1 Heat treatment process conditions

Process	Factor	Unit	Level	Remarks
High temp. (anneaing)	Temp.(HT)	°C	1,100	Fix
	Amount of hydrogen (HH)	cc	2,000 3,000	2 Level
	Velocity(HV)	mm/min	15 / 20	2 Level
Low temp. (ordering)	Temp.(LT)	°C	475 485 495 505 515	5 Level
	Amount of hydrogen(LH)	cc	2,000	Fix
	Velocity(LV)	mm/min	20	Fix

Table 1 presents the heat treatment process conditions. The factorial design of DOE was used to apply the process variables, such as belt speed, hydrogen concentration, and low temperature, in the low-temperature heat treatment process [10-12]. The experiments were repeated to establish 40 types of experimental plans.

2.3 Output Characteristic Measurement Method

For the output characteristics, the characteristic changes caused by temperature and over current were measured. To analyze the output characteristics according to the temperature change around the material, measurements were conducted using a chamber. The room temperature was set to 25 °C, low temperature was set to -20 °C, and high temperature was set to 70 °C. After maintaining the temperature for 1 h to enable a stable state to be established, the output characteristics were measured at this state. The results were expressed in percentage in comparison with those at room temperature. This was set in consideration of the temperature range in which the material would actually be used in the product. The over-leakage characteristic refers to the degree to which the characteristic varies after a large current is applied to the product. In this study, the DC current was applied to the material to saturate the material, and the output change of the sensor due to the residual magnetic flux density was measured for the analysis of the over-leakage characteristics. The difference was calculated as a percentage by comparing the measured value upon application of the overvoltage of 10 A to the sample for 1 min through the DC power supply, and the measured value at room temperature.

A specimen was prepared from the iron core, and a circuit diagram was constructed to measure the electrical output characteristics through the excitation characteristics of the specimen. The electrical properties were measured by applying a magnetic field to the primary side to excite the material, and the material was wound to measure the voltage induced on the secondary side according to the applied current. To apply the excitation current to the iron core, the input current was set to 20 mA, and the frequency was set to 60 Hz using the AC voltage standard to apply a magnetic field to the material. The induced magnetic flux density flowed to the secondary side wound in the form of voltage. For this, the iron core-shaped material was placed in the case and wound to 1,000 turns with a urethane copper wire of 0.1 Φ, and the voltage induced therein was measured. The induced voltage on the secondary side was recorded via a digital multimeter. After setting the multimeter to measure the AC voltage in mV, the induced voltage was measured. In the measurement, the multimeter was calibrated to zero for each sample to minimize the deviation of the measurement.

3. Electrical Characteristic Analysis

3.1 Measurement Results

Table 2 presents the measurement results based on the amount of hydrogen and speed during the high-temperature heat treatment, and temperature

conditions during the low-temperature heat treatment. It presents the measurement results of the low-temperature characteristics, high-temperature characteristics, and over-leakage characteristics according to the process condition based on the results of the 40 experiments.

3.2 Low Temperature Characteristics

The low-temperature characteristic is a percentage representing the difference between the voltage measured at the set temperature of –20 °C and the measured voltage at room temperature. It was analyzed to confirm the stability of the output sensor at low temperatures. The test results confirmed the factors affecting the low-temperature characteristics through variance analysis. The most influential factor on the low-temperature characteristics was found to be the temperature condition during the low-temperature heat treatment process.

Table 3 presents the ANOVA results, and Figure 1 depicts the main effect plot of the low-temperature properties. The main effect analysis graph also shows that it is significantly affected by the temperature of low-temperature heat treatment, followed by the amount of hydrogen at the high-temperature condition.

3.3 High Temperature Characteristics

The high-temperature characteristic is a percentage representing the difference between the voltage measured at the set temperature of 70 °C and that at room temperature. It was analyzed to confirm the stability of the output sensor at high temperatures. The test results confirmed the factors affecting the high-temperature characteristics through variance analysis. Table 4 presents the ANOVA results, and Figure 2 depicts the main effect plot of the high-temperature properties.

Table 2 Measurement results according to process conditions

No	HH	HV	LT	Low-temp. properties (%)		High-temp. properties (%)		Electric leakage properties (%)	
1	2,000	15	475	0.96	1.30	0.77	0.78	-3.01	2.91
2	2,000	15	485	1.45	2.04	0.06	0.19	-1.96	-2.17
3	2,000	15	495	2.26	2.62	0.00	0.12	-0.57	-0.56
4	2,000	15	505	2.57	1.98	-0.13	-0.31	-0.38	-0.44
5	2,000	15	515	1.72	2.19	-0.55	0.63	-0.98	-0.75
6	2,000	20	475	1.08	0.45	0.13	0.45	-2.54	-2.88
7	2,000	20	485	1.63	1.01	0.06	0.25	-1.95	-0.88
8	2,000	20	495	2.05	1.69	-0.19	-0.06	-1.18	-0.75
9	2,000	20	505	2.17	1.93	-0.25	-0.37	-0.74	-0.50
10	2,000	20	515	1.47	1.75	-0.49	-0.81	-0.86	-0.69
11	3,000	15	475	-2.54	0.65	-3.05	0.58	-5.65	-2.97
12	3,000	15	485	1.75	2.77	0.52	0.84	-2.20	-0.51
13	3,000	15	495	1.91	2.19	-0.38	-0.06	-1.46	-0.94
14	3,000	15	505	2.17	1.98	-0.31	0.00	-0.31	-1.30
15	3,000	15	515	0.37	1.42	-0.49	0.00	0.37	0.56
16	3,000	20	475	0.90	0.84	0.45	1.03	-2.58	-2.31
17	3,000	20	485	1.77	1.58	0.25	0.25	-1.71	-1.14
18	3,000	20	495	2.30	1.83	-0.44	-0.13	-1.62	-1.70
19	3,000	20	505	2.53	2.44	0.25	1.06	0.00	0.00
20	3,000	20	515	1.39	0.70	-0.32	-1.08	-0.51	-0.89

Table 3 ANOVA of low temperature properties

Source	DF	Adj SS	Adj MS	F-Value	P-Value
Model	6	16.9158	2.81930	6.08	0.000
Linear	6	16.9158	2.81930	6.08	0.000
HH	1	0.7209	0.72092	1.56	0.221
HV	1	0.0016	0.00156	0.00	0.954
LT	4	16.1933	4.04833	8.74	0.000
Error	33	15.2928	0.46342		
Lack of fit	13	7.5990	0.58454	1.52	0.194
Pure error	20	7.6937	0.38469		
Total	39	32.2086			

Model summary			
S	R-sq	R-sq(adj)	R-sq(pred)
0.680748	52.52%	43.89%	30.24%

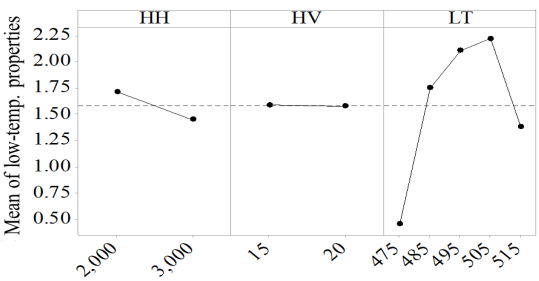

Fig. 1 Main effect plot of low-temp. properties

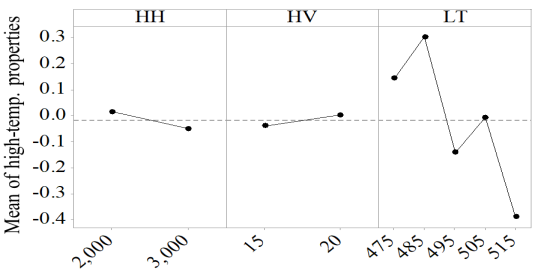

Fig. 2 Main effect plot of high-temp. properties

The main effect analysis graph also confirms that it is significantly affected by the temperature of the low-temperature heat treatment, similar to the case for the low-temperature characteristic. As a result of the variance analysis, the P-value indicates that there is no significant effect on all three factors.

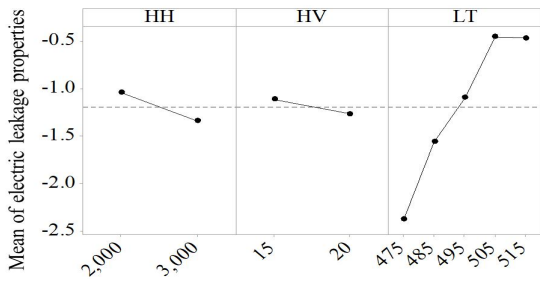

Fig. 3 Main effect plot of electric leakage properties

3.4 Over-leakage Characteristics

The over-leakage characteristic is a result of assuming that a large current is applied to the product. This is similar to the low and high temperatures analyzed earlier. Over-leakage characteristics are also affected by LT, while the other factors appear to be insignificant. Table 5 presents the ANOVA results of the over-leakage property analysis, and Figure 3 depicts the main effect plot of the electric leakage properties.

4. Deriving Optimal Conditions

4.1 Deriving Optimal Conditions

Based on the results obtained through DOE factorial regression, response optimization was used to

Table 4 ANOVA of high temperature properties

Source	DF	Adj SS	Adj MS	F-Value	P-Value
Model	6	2.3125	0.38541	0.78	0.592
Linear	6	2.3125	0.38541	0.78	0.592
HH	1	0.0429	0.04290	0.09	0.770
HV	1	0.0172	0.01722	0.03	0.853
LT	4	2.2523	0.56309	1.14	0.355
Error	33	16.3150	0.49439		
Lack of fit	13	7.7587	0.59682	1.40	0.244
Pure error	20	8.5562	0.42781		
Total	39	18.6274			
Model summary					
S	R-sq		R-sq(adj)		R-sq(pred)
0.703131	12.41%		0.00%		0.00%

Table 5 ANOVA of electric leakage properties

Source	DF	Adj SS	Adj MS	F-Value	P-Value
Model	6	22.0761	3.6794	2.60	0.036
Linear	6	22.0761	3.6794	2.60	0.036
HH	1	0.8970	0.8970	0.63	0.431
HV	1	0.2418	0.2418	0.17	0.682
LT	4	20.9373	5.2343	3.70	0.013
Error	33	46.6696	1.4142		
Lack of fit	13	22.3933	1.7226	1.42	0.234
Pure error	20	24.2763	1.2138		
Total	39	68.7457			
Model summary					
S	R-sq		R-sq(adj)		R-sq(pred)
1.18921	32.11%		19.77%		0.26%

derive the conditions: belt speed of 15 mm/min and hydrogen input of 3,000 Nℓ/h for the high-temperature heat treatment (annealing); and a temperature of 475 °C for the low-temperature heat treatment (ordering). The target values of the low-temperature characteristics, high-temperature characteristics, and over-leakage characteristics were set to zero.

The reason for the target value being set to 0 is that the measured characteristic value represents the difference from the steady state in terms of percentage. Therefore, the closer it is to 0, the closer it is to the steady state.

The conditions are then derived; for the derived conditions, the estimated value of the low-temperature characteristic was 0.327, that of the high-temperature characteristic was 0.089, and that of the over-leakage characteristic was -2.4508. Figure 4 is an optimization graph that depicts the optimal conditions and estimations derived using response optimization.

4.2 Validation

Further experiments were conducted to verify the validity of the derived conditions. The estimated and experimental values were compared using the optimal process conditions derived above. As a result of the

validation test, the estimated low-temperature characteristic was 0.33%, whereas the experimental value was 0.5%, resulting in an error rate of approximately 0.2%.

The estimated high-temperature characteristic was 0.09%, whereas the experimental value was 0.00%, resulting in an error rate of 0.09%. The estimated over-leakage temperature characteristic was -2.45%, whereas the experimental value was -3.03%, resulting in an error rate of approximately 0.6%.

Table 6 The optimal conditions

Process	Temp.	Velocity	Amount of Hydrogen
High temp. (annealing)	1,100 ℃	15 mm/min	3,000 cc
Low temp. (ordering)	475 ℃	20 mm/min	2,000 cc

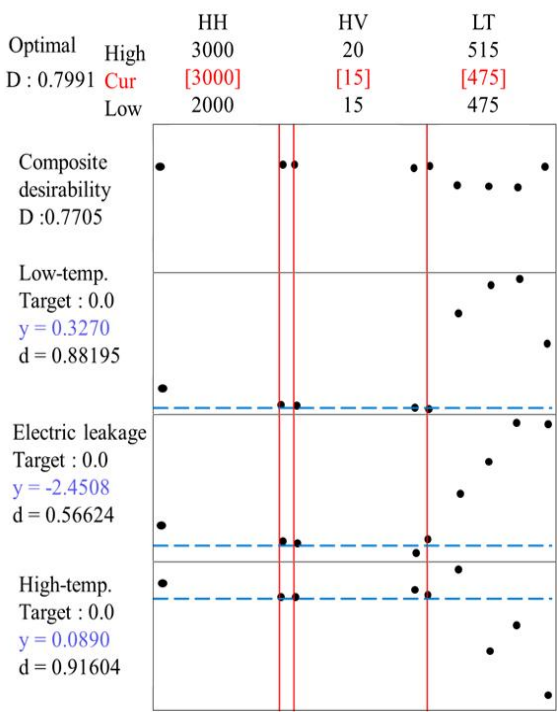

Fig. 4 Optimization plot

Table 7 Comparison of estimated and experimental values

	Low-temp. properties	high-temp. properties	Electric leakage properties
Estimation value	0.33 %	0.09 %	-2.45 %
Experimental value	0.50 %	0.00 %	-3.03 %
error rate	0.17 %	0.09 %	0.58 %

5. Conclusion

In this study, the temperature characteristics and over-leakage characteristics of the Permalloy cores were investigated according to heat treatment conditions to stabilize the output characteristics of the current sensor, and the optimization of the process variables for characteristic values was conducted. To confirm the correlation of the output characteristics according to the heat treatment conditions, the effects of each factor were confirmed through the DOE using the high-temperature and low-temperature heat treatment conditions as the process variables. Specimen fabrication and output characteristic tests were performed according to the Permalloy core hydrogen reduction heat treatment process variables. It was confirmed that the temperature in the furnace during the low-temperature heat treatment was the main factor affecting the characteristic value. Moreover, the optimal conditions were derived to determine the condition to minimize the error rate. Finally, further experiments were conducted to validate the results.

References

1. Zhang, C., Yang, F., Ke, X., Liu, Z. and Yuan, C., "Predictive modeling of energy consumption and greenhouse gas emissions from autonomous electric vehicle operations," Applied Energy, Vol.

38, 2019.
2. Naumanen, M., Uusitalo, T., Huttunen-Saarivirta, E. and van der Have., R., “Development strategies for heavy duty electric battery vehicles: Comparison between China, EU, Japan and USA. Resources,” Conservation and Recycling, Vol. 151, 2019.
3. Uddin, K., Moore, A. D., Barai, A. and Marco, J., “The effects of high frequency current ripple on electric vehicle battery performance,” Applied Energy, Vol. 178, pp. 142-154, 2016.
4. Lyu, Y., Siddique, A. R. M., Majid, S. H., Biglarbegian, M., Gadsden, S. A. and Mahmud, S., “Electric vehicle battery thermal management system with thermoelectric cooling,” Energy Reports, Vol. 5, pp. 822-827, 2019.
5. Osberger, L., Frick, V. and Hébrard, L., “High resolution shallow vertical Hall sensor operated with four-phase bi-current spinning current,” Sensors and Actuators A: Physical, Vol. 244, pp. 270-276, 2016.
6. Yatchev, I., Sen, M., Balabozov, I. and Kostov, I., “Modelling of a Hall effect-based current sensor with an open core magnetic concentrator,” Sensors, Vol. 18, No. 4, pp. 1260, 2018.
7. Girgin, A., Bilmez, M., Amin, H. Y. and Karalar, T. C., “A silicon Hall sensor SoC for current sensors,” Microelectronics Journal, Vol. 90, pp. 12-18, 2019.
8. Yeon, K., Kim, S. and Son, D., “Construction of Current Sensor Using Hall Sensor and Magnetic Core for the Electric and Hybrid Vehicle,” Journal of the Korean Magnetics Society, Vol. 23, No. 2, pp. 49-53, 2016.
9. Lei, J., Lei, C. and Zhou, Y., “Analysis and comparison of the performance of MEMS fluxgate sensors with permalloy magnetic cores of different structures,” Measurement, Vol. 46, No. 1, pp. 710-715, 2013.
10. Hößler, D. and Ernst, M., “Optimization of a TiSi2 formation based on PECVD Ti using DoE methodology,” Solid-State Electronics, Vol. 158. pp. 51-58, 2019.
11. Yongfan, L., Shuai, Z. and Jing. W., “Research on the Optimization Design of Motorcycle Engine Based on DOE Methodology,” Procedia Engineering, Vol. 174, pp. 740-747, 2017.
12. Lee, C., Sa, M. and Kim. J., “Fabrication of 3D Bioceramic Scaffolds using Laser Sintering Deposition System and Design of Experiment,” Journal of the Korean Society of Manufacturing Process Engineers, Vol. 18, No. 12, pp. 59-66, 2019.